Energy 231 (2021) 121069

Contents lists available at ScienceDirect

Energy

journal homepage: www.elsevier.com/locate/energy

Effects of injection timing and EGR on combustion and emissions characteristics of the diesel engine fuelled with acetone–butanol–ethanol/diesel blend fuels

Xiongbo Duan [a], Zhengxin Xu [b, c, *], Xingyu Sun [a], Banglin Deng [b], Jingping Liu [a]

[a] State Key Laboratory of Advanced Design and Manufacturing for Vehicle Body, Hunan University, Changsha, 410082, China
[b] College of Mechatronics and Control Engineering, Shenzhen University, Shenzhen, 518060, China
[c] Key Laboratory of Optoelectronic Devices and Systems of Ministry of Education and Guangdong Province, College of Optoelectronic Engineering, Shenzhen University, Shenzhen, 518060, China

ARTICLE INFO

Article history:
Received 26 December 2020
Received in revised form
14 May 2021
Accepted 24 May 2021
Available online 28 May 2021

Keywords:
Acetone–butanol–ethanol
Injection timing
EGR
Combustion
Emission
Diesel engine

ABSTRACT

The acetone–butanol–ethanol (ABE) is the intermediate product during the bio-butanol fermentation process, and is widely considered as one of the promising alternative fuels in the diesel engine for its advantages of oxygenated fuels, better air–fuel mixing, lower NOx and soot emissions, and lower production cost. In this paper, different ABE ratios in the diesel fuel and injection timings were tested in the AVL diesel engine, and obtained the combustion and emission characteristics parameters for the late model calibration. Then, the CFD KIVA-3V code coupled with the CANTERA code was built and validated against the experimental data. Subsequently, different injection timings and exhaust gas recirculation (EGR) ratios were investigated on the diesel engine fuelled with the ABE/diesel blended fuel to unveil their effects on the combustion and emissions behaviors. The results indicated that the injection timing and EGR strongly affected the combustion process of the diesel engine fuelled with the ABE/diesel fuel. In addition, the oxidation and formation process of the intermediate species, soot precursors, final soot, NOx, CO and HC emissions in the diesel engine fuelled with the ABE/diesel fuel were also significantly impacted by the injection timing and EGR strategies.

1. Introduction

With increasing ecological and environmental concerns of the traditional fossil fuels and stringent exhaust emission regulations [1–3], the engine community and auto makers paid more attention to the renewable energy for the future generation engines [4–6], such as the Atkinson cycle engine [7] and homogeneous charge compression ignition (HCCI) engine [8,9]. In addition, the next generation of biofuels could be made from the renewable sources and agricultural waste materials (such as cornstalks and wheat shafts) [10], which show the exciting possibility and promising of renewability in the sense that the biofuels could be thoroughly regenerated by the ecosystem and completely realized a dynamic balance between the carbon source and carbon sink by using the combustion products of the fuels [11,12]. Currently, the alcohol fuels, such as methanol [13], ethanol [14,15], butanol [16], etc. are being widely tested and used as possible replacements or additions for the internal combustion engine (ICE) [17], which greatly alleviate dependence on the conventional fossil fuels as an energy source for passenger and transportation vehicles.

Among these alcohol fuels, butanol is considered a promising alternative fuel for partially substituting or totally replacing the diesel fuel due to its superior physic-chemical properties, which has higher heating value and cetane number (CN), lower auto-ignition temperature and evaporation pressure, less hygroscopic performance and higher miscibility than the popular methanol and ethanol [18]. Technically, there are two main ways to produce the butanol. The one is produced from the traditional fossil fuel (petro-butanol) through the synthetic petrochemical reactions. While the other one is generated from the biomass (bio-butanol) by the fermentation of carbohydrates, such as sugarcane, bagasse, and other non-food feedstock. Currently, the pretro-butanol is still converted from the fossil fuel and its production cost is strongly

* Corresponding author. College of Mechatronics and Control Engineering, Shenzhen University, Shenzhen, 518060, China.
E-mail address: zhengxin.xu@hotmail.com (Z. Xu).

https://doi.org/10.1016/j.energy.2021.121069
0360-5442/

depended on the price of the crude oil, which obviously indicates that this method is not best solution for reducing the carbon emissions and alleviating the energy crisis [19]. The bio-butanol could be obtained through the fermentation of carbohydrates using the Clostridium strains, which produces the target butanol and other acetone, ethanol and water at the same time [20,21]. Therefore, in order to get the purified butanol, the mixture of the acetone, ethanol and water in the solvent needs to be further removed by using distillation [22]. However, the cost of obtaining the pure butanol from the fermentation broth of acetone-butanol-ethanol (ABE) mixture is high when using the distillation due to its boiling point of 118 °C [11], thereby limiting the production of commercial butanol on a large scale. Moreover, the quantity and productivity of the butanol from the ABE fermentation broth are exceptionally low. However, instead of separating out the butanol from the broth, the ABE mixture could be directly used or blended with diesel fuel in the engine as the bio-fuel [23], which would significantly decrease the additional cost of butanol distillation and could be distributed through the existing fuel infrastructure [24], thereby allowing to be commercially used in the diesel engine.

Generally, the ABE is the intermediate product of biobutanol production with a specific volumetric ratio of the 3: 6:1 during the fermentation process [25,26]. In addition, the alternative fuel of ABE will have a relatively higher oxygen content, which is conducive to decrease the global equivalence ratio during the spray combustion in the cylinder. The presence of the chemically bounded oxygen in the ABE fuel benefits to enhance the combustion efficiency, resulting in decreasing the soot precursor formation and oxidation during the combustion process. Technically, soot emissions formation in the cylinder of the engine are primarily consists of the different carbon components, including the elemental carbon, organic carbon, and carbonate carbon [27]. Moreover, the mechanisms of the nucleation and growth of incipient soot particles in the cylinder are initiated from the polycyclic aromatic hydrocarbons (PAHs), and extensively studied by the experiments and simulations [28,29]. Most PAHs mechanisms in the literature, their main reaction pathways for benzene formation conclude the recombination reaction of propargyl radical (C_3H_3) and other reactions among C_2H_x, C_3H_y and C_4H_z [30]. The cyclopentadiene (C_5H_5) is one of the very important intermediate species in the oxidation of aromatic compounds [31], and would combined with the methyl (CH_3) to form benzene rings in another important pathway. Therefore, the PAHs formation process would be formed the naphthalene, phenanthrene, pyrene, coronene, ovalene and anthracene, etc. through the nucleation, grow and aggregation steps. Subsequently, the ABE blended with the diesel fuel would definitely exert a significant influence in the soot precursor and the final soot formation and oxidation in the diesel engine. Some researchers have already studied the combustion and soot behaviors of the diesel engine fuelled with the ABE/diesel blended fuels, and showed some promising results in the literature through the experimental and numerical investigation [32]. The most obvious advantages of the combustion characteristics of ABE-diesel in the diesel engine are contained the higher oxygen content and latent heat of vaporization, which significantly reduces the soot precursor formation and promotes the final soot oxidation compared to pure diesel. In addition, the longer ignition delay period and flame lift-off length could allow more air entrainment upstream during the spray. At the same time, the ABE-diesel blended fuels contain different types of species and show different volatilities, which would trigger the micro-explosion during the spray [33], and thereby providing better air–fuel mixing [34]. Furthermore, using the ABE in the diesel engine as alternative fuel could achieve the low temperature combustion (LTC) and avoid the high temperature region in the equivalence ratio and temperature (φ-T) map [35,36], which is beneficial to greatly decrease the nitrogen oxide (NOx) emissions formation in the cylinder. Generally, the LTC strategy used in the diesel engine could be realized through using a large amount of exhaust gas recirculation (EGR) or adopting injection strategy.

In this paper, the goal is to study the combustion and emissions characteristics of the diesel engine fuelled with the ABE/diesel blended fuels and hence used as an alternative fuel for diesel engine in real applications. This paper is structured in the following manner. First, different ABE ratios in the diesel fuel and different injection timings were tested in the AVL diesel engine, and obtained the combustion and the emissions data for the late model calibration. Then, the CFD KIVA-3V code coupled with the CANTERA code was built, validated against the experimental data, and finally employed the calibrated model in this paper for simulating the combustion process and the formation and oxidation processes of the soot precursors and final soot emissions. Last, different injection timings and different EGR ratios were investigated on the diesel engine fuelled with the ABE/diesel blended fuel to unveil their effects on the combustion and emissions behaviors. The novelty of this work mainly lay in the following two aspects. First, the simulation platform of the CFD KIVA-3V code coupled with the CANTERA code was built, and used to calibrate the diesel engine fuelled with the ABE/diesel blend fuels. Second, the reduced combustion mechanism of the toluene reference fuel (TRF), ABE and PAH was used to predict the combustion process and the formation and oxidation processes of the soot precursors (acetylene, phenanthrene and pyrene, etc.) and final soot emissions.

2. Experiment setup

2.1. Test engine and rigs

The single-cylinder diesel engine was used in this study and conducted a series of experiments. The main technical parameters of this diesel engine are listed in Table 1. Specifically, the bore and stroke of the test engine are 85 mm and 90 mm, respectively. The displacement of the test engine is 510.7 cm^3 and its compression ratio is 17.1. The Bosch high-pressure common rail injection system CP3 was used in the experiment, which could provide the injection pressure of 40–80 MPa. In addition, the fuel injection system was controlled by the open electronic control unit (ECU). The ETAS ES580 electronic calibration system and the ETAS INCA could manually adjust the parameters, such as the injection timing, injection profile and injection pressure. Fig. 1 illustrates the schematic diagram of the single-cylinder diesel engine on the test bench, which included the dynamometer, fuel injection system, exhaust

Table 1
The main technical parameters of the diesel engine.

Parameter	Value
Engine type	Single-cylinder, four-stroke
Bore (mm)	85
stroke (mm)	90
Displacement (L)	0.51
Geometric compression ratio	17.1
Rated power (kW)/Speed (rpm)	60/4200
Fuel injection mode	Direct injection
Fuel injection system	Bosch high pressure common rail
Nozzle hole (–)	5
Nozzle diameter (mm)	0.18
Nozzle angle (°)	142
Injection pressure (MPa)	60
Intake valve close (°CA ATDC)	−134
Exhaust valve open (°CA ATDC)	128
Fuel type	Diesel and diesel/ABE blend

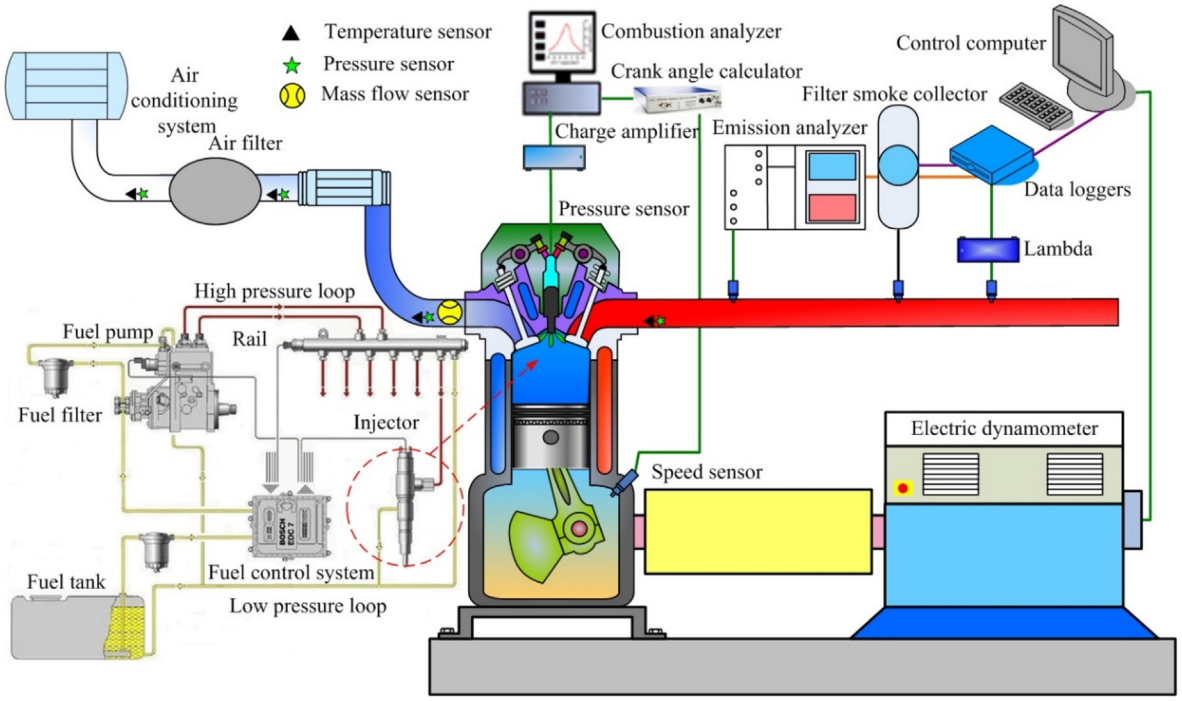

Fig. 1. Schematic of the experimental setup system.

emission analyzer, data acquisition system and combustion analyzer. The high-frequency quartz pressure transducer (Kistler 6121) was mounted in the cylinder of the test engine and recorded the in-cylinder pressure, which could obtain the heat release rate according to the first law of thermodynamics [37]. The sampling probe was installed into the exhaust pipe to collect the exhaust gases and imported into the emission analyzer. For example, the NOx emissions were measured by using the Horiba MEXA-720 emission analyzer, while the hydrocarbon (HC) and carbon dioxide (CO) emissions were measured by the Horiba MEXA-554JU emission analyzer. The soot emissions were measured by the standard filter paper in this study. During the test process, the DV-85 N vacuum pump was used to sample the original exhaust gas through 7/8 circular filter paper. In addition, the McMaster linear filter was installed after vacuum pump to remove oil or water. The sampling flow was monitored and controlled by a flow meter located at the inlet of the vacuum pump, which has a maximum air flow of 2349 L/h under the standard conditions. The air/fuel ratio was measured by the lambda meter, which was coupled with a wide-range oxygen sensor and sent to the open ECU as feedback information. The exhaust port temperature was directly measure by the K-type thermocouple sensor in the exhaust pipe, while the intake port temperature was measured by the Pt-100 low-temperature sensor. During the experiments, the outlet coolant temperature of the test diesel engine was maintained at 88 ± 2 °C by the coolant conditioning system.

2.2. Test fuel samples and operating conditions

The ultra-low sulfur diesel (ULSD) and the ABE/diesel blend fuels were used in the AVL diesel engine. It is noted that the ABE used in this paper was mixed by the acetone, butanol, and ethanol with the volumetric ratio of 3:6:1 to simulate the ABE fermentation product. In addition, the pure diesel was treated as the baseline test fuel and named the D100 in this paper. Then the ABE was mixed with the pure diesel and stored in different containers before the experiments. The volume ratios of the ABE and pure diesel were set at 10:90 and 20:80, which were referred to the ABE10 and ABE20, respectively. The physicochemical properties of the diesel, acetone, butanol, ethanol, ABE10 and ABE20 are listed in Table 2. Table 3 presents the key boundary conditions for the diesel engine. During the experiments, the speed of the diesel engine was fixed at 1200 r/min, the inlet air pressure was set at 1.0 bar, and the inlet air temperature was maintained at 330 K by the air condition system. In addition, the fuel injection pressure was set at 60 MPa and the fuel mass per cycle was 15 mg. Lastly, the test diesel engine was fuelled with the D100, ABE10 and ABE20 under the injection timing of −4°CA ATDC and −8°CA ATDC, respectively. Meanwhile, the in-cylinder pressure, soot, NOx, CO and HC emissions were collected simultaneously after the test diesel engine operated stably for a while.

3. Simulation setup and validation

3.1. Simulation setup

In this study, the AVL diesel engine was used to perform the experiments, and test different ABE ratios in diesel fuel and different injection timings. The original injector was assembled with five holes and distributed symmetrically. Thus, in order to save computational cost and simulation timing, 72° sector computational domain was selected to conduct the simulation cases. Moreover, the grid size independence was also conducted on this simulation model. Furthermore, the simulation process was calculated from the intake valve closing (IVC) −134°CA after top dead center (ATDC) to the exhaust valve opening (EVO) 128°CA ATDC, which included the compression stroke, fuel injection, combustion process and power stroke. Fig. 2 illustrates the computing grid at the top dead center (TDC).

The CFD KIVA-3V Release 2 code [40] was coupled with the open-source CANTERA chemical kinetics code [41] by replacing the KIVA default chemical subroutines to model the thermodynamic

Table 2
The physicochemical properities of the diesel, acetone, butanol, ethanol, ABE10 and ABE20 [14,38,39].

Properties	Diesel	Acetone	Butanol	Ethanol	ABE 10	ABE 20
Molecular formula	C_{12}–C_{25}	C_3H_6O	nC_4H_9OH	C_2H_5OH	–	–
Cetane number	40	–	25	8	–	–
Oxygen content (wt. %)	–	27.6	21.6	34.8	2.37	4.77
Density at 15 °C (g/mL)	0.82–0.86	0.791	0.813	0.795	0.837	0.833
Auto-ignition temperature (°C)	230	560	385	434	–	–
Lower heating value (MJ/kg)	42.7	29.6	33.1	26.8	41.62	40.53
Boiling point (°C)	282–338	56.1	117.7	78.3	–	–
Stoichiometric ratio (–)	14.3	9.54	11.21	9.02	13.93	13.57
Latent heat at 25 °C (kJ/kg)	270	518	582	904	301.3	332.8
Flammability limits (vol. %)	0.6–5.6	2.6–12.8	1.4–11.2	3.3–19	–	–
Saturation pressure at 38 °C (kPa)	0.3	53.4	2.27	13.8	–	–
Viscosity at 40 °C (mm^2/s)	1.9–4.1	0.35	2.63	1.08	–	–

Table 3
Key boundary conditions for the diesel engine.

Item	Content
Engine speed (r/min)	1200
Fuel type (–)	D100, ABE10, ABE20
Fuel mass per cycle (mg)	15
Injection pressure (MPa)	60
Injection timing (°)	142
Injection timing (°CA ATDC)	−8, −4
Intake pressure (bar)	1.0
Intake temperature (K)	330
Intake valve close (°CA ATDC)	−134
Exhaust valve open (°CA ATDC)	128

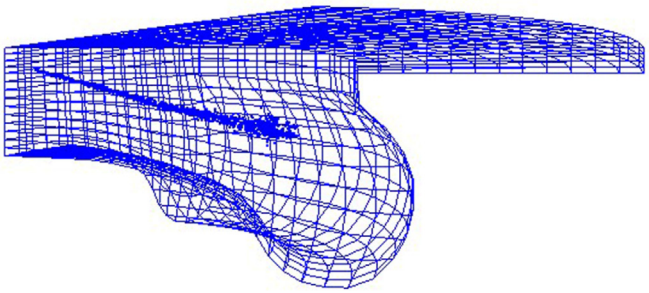

Fig. 2. Computational domain for the test diesel engine.

data, such as the species compositions and internal energy in our previous paper [42]. Specifically, the KIVA was utilized to directly calculate the mass, momentum, and energy conservation equations, while the CANTERA was used to simulate the chemical kinetics, thermodynamics, and transport processes. In other words, the CANTERA solver was adopted to process the chemistry calculation in each computational cell, which was generally assumed as an adiabatic and constant-volume homogeneous system, while the fluid flow and combustion processes were calculated by the KIVA code. In addition, several physical sub-models were selected during the three-dimensional (3-D) simulation by computational fluid dynamics (CFD). For example, the Renormalized k-ε model [43] was employed to consider the effects of turbulence on the flow during the simulation. The Taylor Analogy Breakup (TAB) model [44] was used to process the spray atomization and droplet breakup, while the O'Rourke model was utilized to model the spray droplet collision [45]. Furthermore, a multi-component evaporation model developed by Zeng and Lee [46] was also implemented during the simulation in order to consider the evaporation of multicomponent droplets, particularly the diesel-ABE blend fuels in this study. The reduced combustion mechanism of the toluene reference fuel (TRF), ABE and PAH was developed in our previous paper [42], which contained 98 species and 456 reactions. In addition, the extended Zeldovich mechanism was also embedded into this reduced combustion mechanism for the prediction of the NOx formation. Some reactions and related species for acetone, n-butanol and ethanol were also included in this reduced combustion mechanism in order to enhance the ignition behavior of ABE/diesel blends at the low temperature. Moreover, this reduced combustion mechanism predicted the laminar flame speed and the species profiles in the jet-stirred reactors (JSR), which could be used to investigate the combustion and emission characteristics of the diesel engine fuelled with ABE/diesel blend fuels.

Table 4 lists the key boundary conditions for the diesel engine CFD simulation cases calibration. In this study, different types of fuels (D100, ABE10 and ABE20) and different injection timings (−4°CA ATDC and −8°CA ATDC) were selected for validating the simulation model according to the experimental data. The first and second simulation cases (Case #1 and Case #2) were used the pure diesel (D100) as the baseline case, which were mixture of the toluene/n-heptane with a volume ratio of 20%/80% and used as the alternative fuels. The others simulation cases (Case #3 to Case #6) were separately used the blends of the ABE and diesel with a volume ratio of 10%/90% (ABE10) and 20%/80% (ABE20) under the injection timing of −4°CA ATDC and −8°CA ATDC. During the simulation calculation, the speed of the diesel engine was maintained at 1200 r/min, the inlet air pressure was fixed at 1.0 bar, and the inlet air temperature was kept at 330 K. In addition, the fuel injection pressure was set at 60 MPa and the fuel mass per cycle was 15 mg. Furthermore, the IVC was set at −134°CA ATDC, and the EVO was set at 128°CA ATDC.

3.2. Model validation

Fig. 3 illustrates the comparison of experimental and simulated in-cylinder pressure and heat release rate (HRR) of the diesel engine fuelled with the D100, ABE10 and ABE20 under the injection timing of −4°CA ATDC and −8°CA ATDC, respectively. As can be seen from Fig. 3, the in-cylinder pressure and heat release rate of the diesel engine were matched with the experimental data very well by using the sector computational domain. Furthermore, the main combustion characteristics, including the ignition delay period, peak combustion pressure and peak heat release rate were also showed a good agreement with the experimental data. In other words, the KIVA-3V coupled with the CANTERA used in this paper could effectively and accurately predict the spray and combustion processes of the diesel engine fuelled with the pure diesel and ABE/diesel blend fuels.

Fig. 4 depicts the comparison of experimental and simulated soot, NOx, CO and HC emissions of the diesel engine fuelled with

Table 4
Key boundary conditions for the diesel engine CFD simulation case calibration.

Item	Case #1	Case #2	Case #3	Case #4	Case #5	Case #6
Engine speed (r/min)	1200	1200	1200	1200	1200	1200
Fuel type (−)	D100	D100	ABE10	ABE10	ABE20	ABE20
Fuel mass per cycle (mg)	15	15	15	15	15	15
Injection pressure (MPa)	60	60	60	60	60	60
Injection angle (°)	142	142	142	142	142	142
Injection timing (°CA aTDC)	−4	−8	−4	−8	−4	−8
Intake pressure (bar)	1.0	1.0	1.0	1.0	1.0	1.0
Intake temperature (K)	330	330	330	330	330	330
Intake valve close (°CA ATDC)	−134	−134	−134	−134	−134	−134
Exhaust valve open (°CA ATDC)	128	128	128	128	128	128

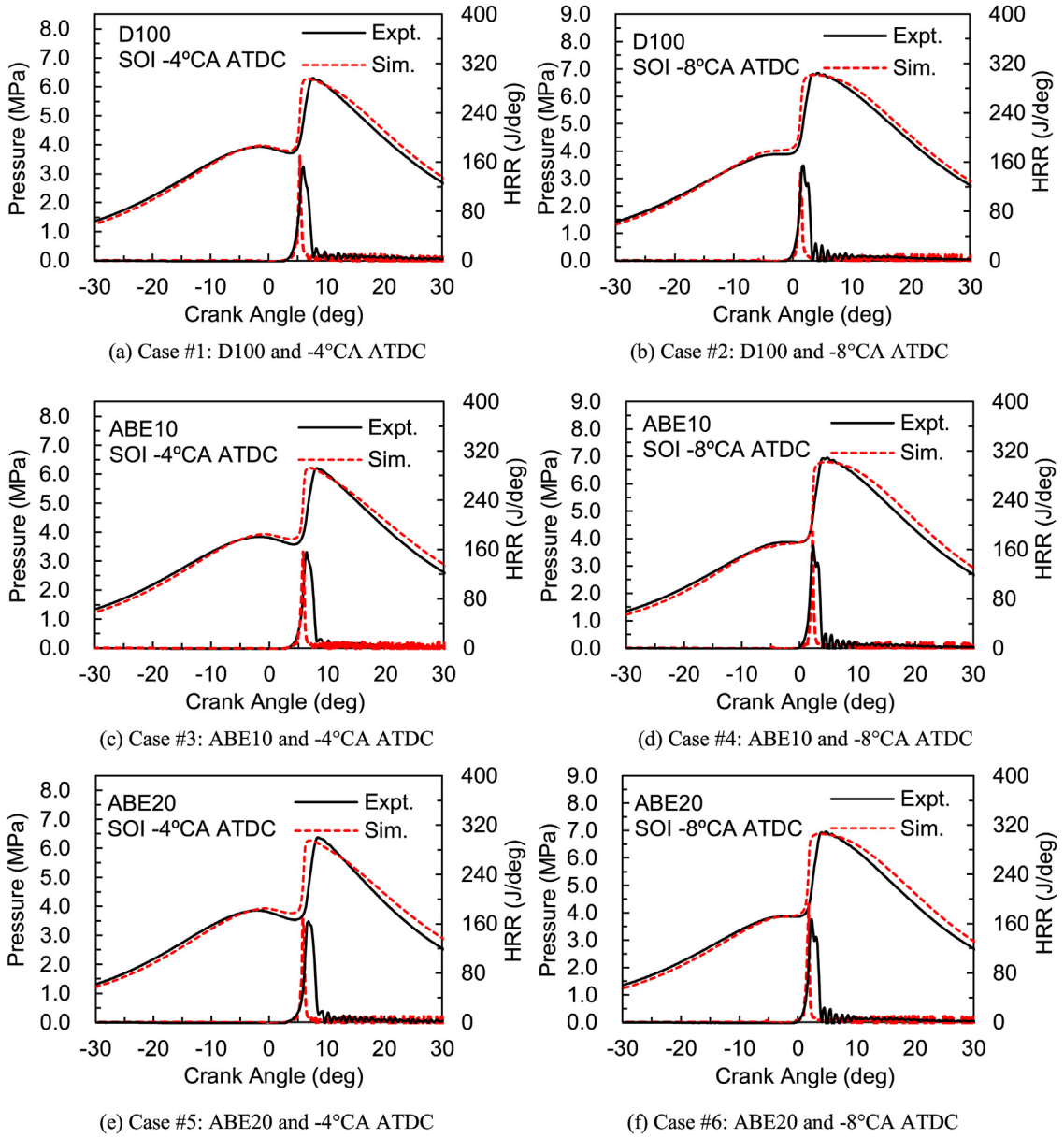

Fig. 3. Comparison of experimental and simulated in-cylinder pressure and heat release rate under different conditions.

the D100, ABE10 and ABE20 under the injection timing of −4°CA ATDC and −8°CA ATDC, respectively. It is noted that the soot mass of the diesel engine fuelled with the ABE/diesel blends were normalized based on the pure diesel. As one can see from Fig. 4, the trends of the soot emissions of the diesel engine fuelled with the D100, ABE10 and ABE 20 were basically consistent with the experimental data under the injection timing of −4°CA ATDC and −8°CA ATDC. Namely, the soot mass decreased with increasing

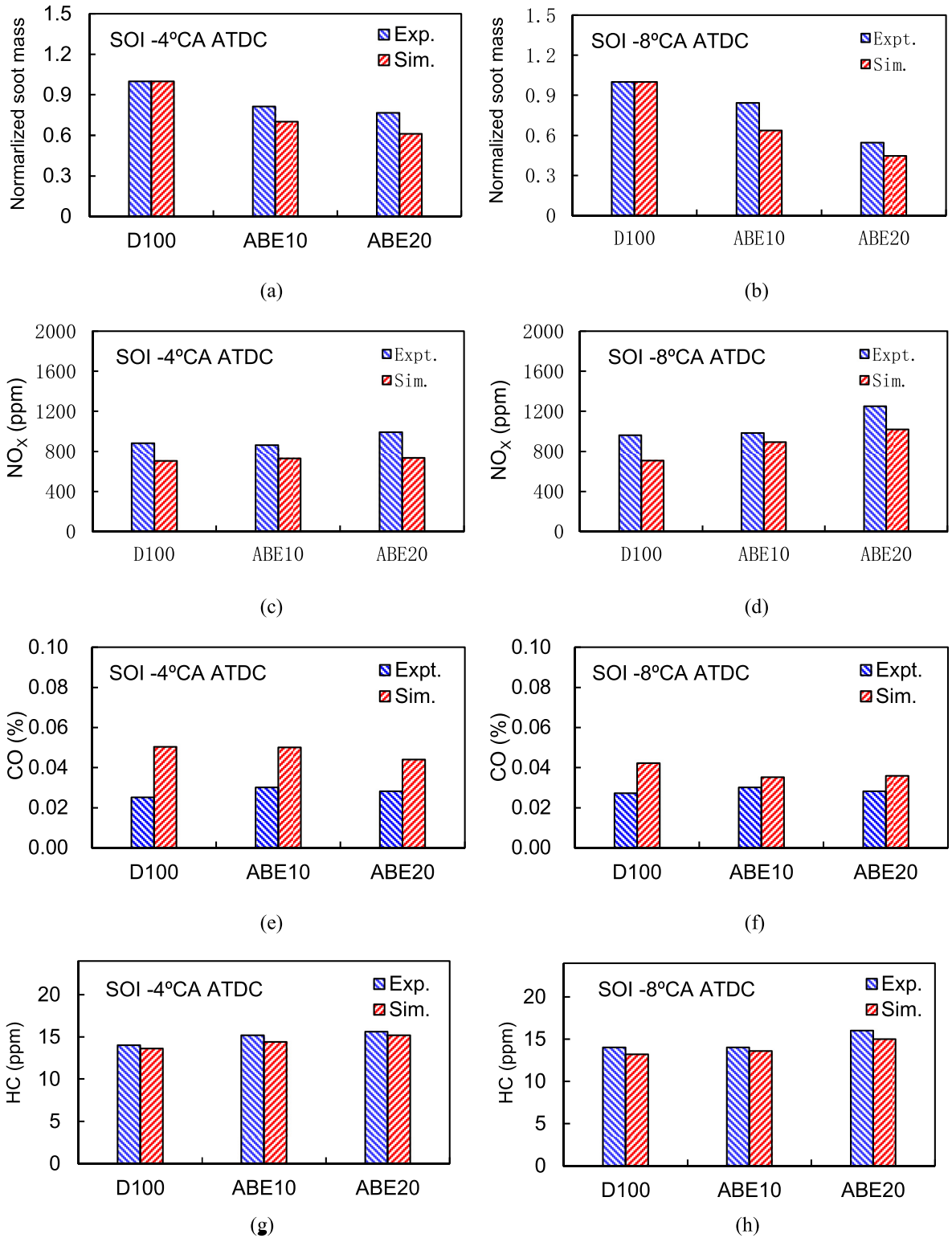

Fig. 4. Comparison of experimental and simulated soot, NOx, CO and HC emissions under different boundary conditions.

the ABE ratio in the diesel under the same operating condition. In addition, the simulated NOx emissions of the diesel engine fuelled with the D100, ABE10 and ABE 20 were slightly lower than that the experimental data, but their trends were in good agreement with the test results. Furthermore, the trends of the CO and HC emissions were also basically consistent with the experimental data. Although, the simulated emissions of the diesel engine fuelled with the D100, ABE10 and ABE20 were not perfectly matched with the experimental data under the injection timing of −4°CA ATDC and −8°CA ATDC, but the platform of the KIVA coupled with the CANTERA still could be used to qualitatively analyze the performance of the engine fuelled with the ABE/diesel blend fuels by

using this reduced combustion mechanism. Obviously, the exhaust emissions of the test engine were decreased with increasing the ABE ratio in the diesel. In addition, as listed in Table 2, the lower heating value of the ABE20 is almost closed to the pure diesel, which means that the output power of the diesel engine fuelled with ABE20 will maintain the same. Consequently, in the next section, the ABE20 was used in the diesel engine to investigate the effects of different injection timings and different EGR ratios (Case #7 to Case #13) on the combustion and emissions characteristics according to Table 5.

4. Results and discussion

4.1. The effects of the injection timing on combustion and emission characteristics of the diesel engine

This section was mainly investigated the effects of different fuel injection timings by sweeping from −8°CA ATDC to −2°CA ATDC on the combustion and emissions characteristics of the diesel engine fuelled with the ABE20. As stated earlier, the ABE20 was the mixture of the diesel and ABE with a specific volume ratio of 20%/80%. In addition, the ABE is the intermediate product of the bio-butanol production during the fermentation process, and its components are the acetone, butanol, and ethanol with the specific volume ratio of 3: 6: 1. Fig. 5 illustrates the in-cylinder pressure, HRR and in-cylinder mean temperature of the diesel engine fuelled with the ABE20 under different injection timings. It can be seen from Fig. 5 (a) that the peak combustion pressure and peak heat release rate of the test diesel engine fuelled with the ABE20 increased with the advance of the fuel injection timing. In addition, the heat release rate was advanced with the earlier injection timing. As can be seen from Fig. 5 (b), the in-cylinder mean temperature was slightly increased with advancing the injection timing. These trends were mainly attributed to the following interactive reasons. With using the earlier injection timing, the ABE20 was directly injected into the cylinder of the diesel engine before the TDC. During this period, the in-cylinder temperature and pressure were relatively lower, which was definitely increased the ignition delay period. During the ignition delay period, more fuel would be atomized and evaporated with the help of the turbulence flow in the cylinder, which meant that more premixed mixture was formed and distributed along the spray process. Once some appropriate premixed mixture reached the auto-ignition temperature during the piston sequentially moved to the TDC, it would burn quickly in multi-place in the cylinder, which could promote the rest of the fuel vaporization and accelerate diffusion combustion. Thus, the heat release of the diesel engine was advanced with using the earlier injection timing. Furthermore, the ratio of the premixed combustion was increased with using the earlier injection timing, which was beneficial to increase the combustion rate, and thereby accelerating the rest of diffusion combustion process. Moreover, more fuel was burned and released heat near the TDC, which was conducive to enhancing the heat-to-work conversion efficiency and built up the peak combustion pressure and temperature in the cylinder. Therefore, the peak combustion pressure and in-cylinder mean temperature were increased with the advance of the injection timing.

Fig. 6 displays the soot, NOx, CO and HC emissions of the diesel engine fuelled with the ABE20 under various injection timings. It can be seen from Fig. 6, the soot mass, CO and HC emissions of the diesel engine fuelled with the ABE20 were decreased with advancing the injection timing, while the NOx emissions were increased with advancing the injection timing. This is largely due to the fact that more available mixing period of the fuel and fresh air obtained with using the earlier injection timing [36], which, of course, benefited to form more premixed mixture and distributed in the cylinder. Therefore, the amount of the hydrocarbon fuels pyrolysis was declined with using the earlier injection timing, which was also beneficial to decrease the soot precursor formation. In addition, more mixture burned through the premixed combustion mode was conducive to decreasing the incomplete combustion, and thereby resulting in relatively lower CO and HC emissions. However, as mentioned earlier, the in-cylinder mean average temperature was increased with advancing the injection timing due to the premixed combustion. Unfortunately, the NOx emissions were favored the combustion temperature, oxygen concentration and reaction time. Consequently, the NOx emissions of the diesel engine fuelled with the ABE20 were increased with using the earlier injection timing.

Fig. 7 depicts the simulated soot, O_2, OH, C_2H_2, phenanthrene (A_3) and pyrene (A_4) of the diesel engine fuelled with the ABE20 under various injection timings. Generally, the soot and intermediate species formation of the test engine were advanced with using the earlier injection timing. Specifically, as shown in Fig. 7 (a), the production rate of the soot and its peak value were slightly increased with the advance of fuel injection timing. However, more premixed mixture was formed in the cylinder and increased the premixed combustion period with using the earlier injection timing, which was beneficial to gradually accelerate the oxidation rate of soot. In addition, with the advancing the injection timing, the combustion would definitely take place earlier in the cylinder, which, of course, consumed the oxygen (O_2) earlier during the combustion process (as displayed in Fig. 7 (b)). Generally, the OH radical was distributed and located along the high combustion temperature of the spray flame. Therefore, as illustrated in Fig. 7 (c), the OH was formed on a large scale with earlier injection timing once the combustion took place in the cylinder after the ignition delay period. Furthermore, according to the phenomenological soot oxidation model improved by the Fenimore and Jones model [47], the OH radical was promoted and accelerated the soot oxidation through the reaction of $C(s) + OH{=}CO + 1/2H_2$. As is known to all, during the soot formation and oxidation processes, there are other

Table 5
Key boundary conditions for the simulation cases on the diesel engine fuelled with ABE20.

Item	Case #7	Case #8	Case #9	Case #10	Case #11	Case #12	Case #13
Engine speed (r/min)	1200	1200	1200	1200	1200	1200	1200
Fuel type (−)	ABE20	ABE20	ABE20	ABE20	ABE20	ABE20	ABE20
Fuel mass per cycle (mg)	15	15	15	15	15	15	15
Injection pressure (MPa)	60	60	60	60	60	60	60
Injection angle (°)	142	142	142	142	142	142	142
Injection timing (°CA aTDC)	−8	−6	−4	−2	−4	−4	−4
EGR ratio (%)	0	0	0	0	15	25	35
Intake pressure (bar)	1.0	1.0	1.0	1.0	1.0	1.0	1.0
Intake temperature (K)	330	330	330	330	330	330	330

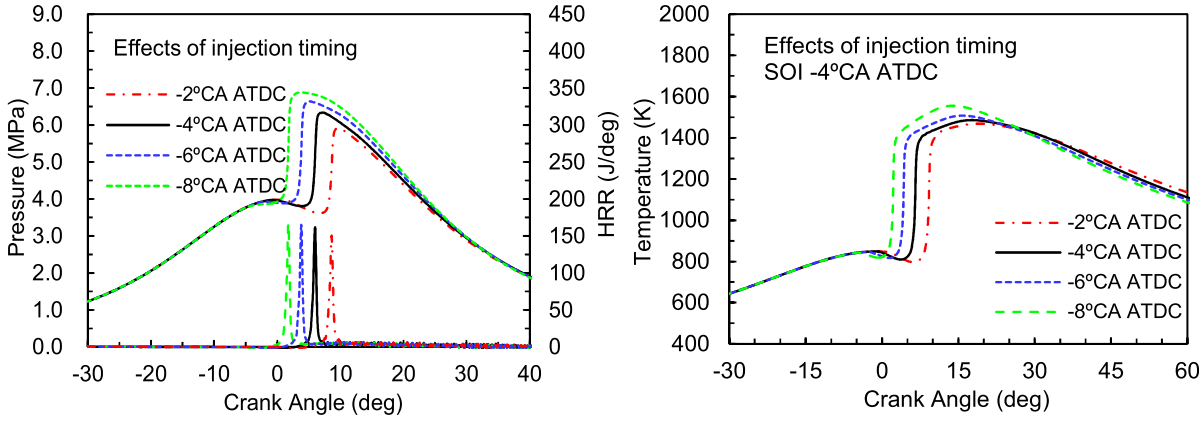

(a) In-cylinder pressure and HRR (b) In-cylinder mean temperature

Fig. 5. The in-cylinder pressure, heat release rate, tempeature of the diesel engine fuelled under various injection timings.

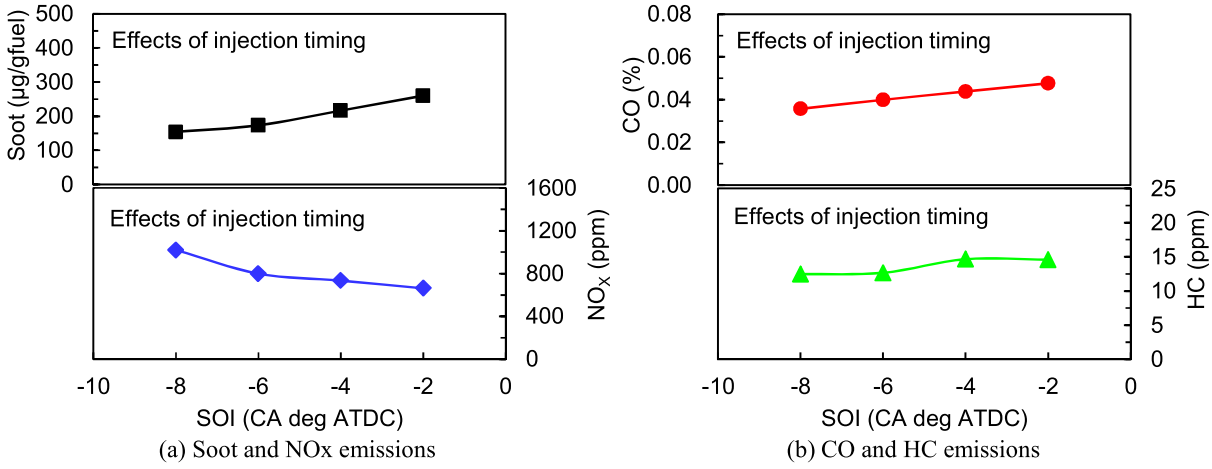

(a) Soot and NOx emissions (b) CO and HC emissions

Fig. 6. The soot, NOx, CO and HC of the diesel engine fuelled with ABE20 under various injection timings.

precursors and intermediate species formation, such as the acetylene (C_2H_2), polycyclic aromatic hydrocarbons, A_3 and A_4 and so on. Then, after a series of complex physical and chemical reaction processes, these precursors and intermediate species led to form the final soot through cyclization, nucleation, coalescence, surface growth and agglomeration. As demonstrated in Fig. 7 (d), (e) and (f), the formation and oxidation of the C_2H_2, A_3 andA_4 were also advanced with using the earlier injection timing. These trends could be explained by following interactive reasons. First, the C_2H_2, A_3 andA_4 were formed once the combustion occurred, and thereby advancing the formation of the precursors. In addition, with using the earlier injection timing, more premixed mixture formed in the cylinder, which was beneficial to increase the ratio of the premixed combustion, and thereby reducing the C_2H_2, A_3 andA_4 formation and accelerating their oxidation.

Fig. 8 shows the simulated temperature, equivalent ratio, OH, NOx and soot distribution in the cylinder of the diesel engine fuelled with the ABE20 under various injection timings. It is noted that these cross-sectional planes were cut at the timing of the peak soot mass formation during the simulation. Apparently, the peak soot mass formation advanced with using the earlier injection timing. As illustrated in Fig. 8 (a), the high combustion temperature regions of the diesel engine fuelled with the ABE20 were located near the piston bowl due to the fuel spray penetration, initial premixed mixture formation, and the late combustion occurred. In addition, with advancing the injection timing, the mixing period of the fuel and fresh air and ignition delay period were prolonged due to the relatively lower temperature and pressure before the piston moved to the TDC. Thus, more premixed mixture formed with using the earlier injection timing, which lead to the equivalent ratio relatively evenly distributed near the piston bowl (as shown in Fig. 8 (b)). In addition, the OH radical was also mainly distributed near the piston bowl and strongly depended on the temperature distribution as demonstrated in Fig. 8 (c). On the one hand, the ratio of the premixed combustion was increased with using the earlier injection timing. On the other hand, the combustion temperature and combustion rate in the premixed combustion mode are higher than that of diffusion combustion mode. Consequently, the OH radical was formed along the high combustion temperature of the spray flame. Moreover, the in-cylinder temperature was increasing with increasing the ratio of the premixed combustion, which resulted in a high level of the NOx formation (as depicted in Fig. 8 (d)) with using the earlier injection timing. As stated earlier, more premixed mixture was formed with using the earlier injection timing, and the ratio of the premixed combustion was increased. Thus, the soot was gradually deceased with the advance of the

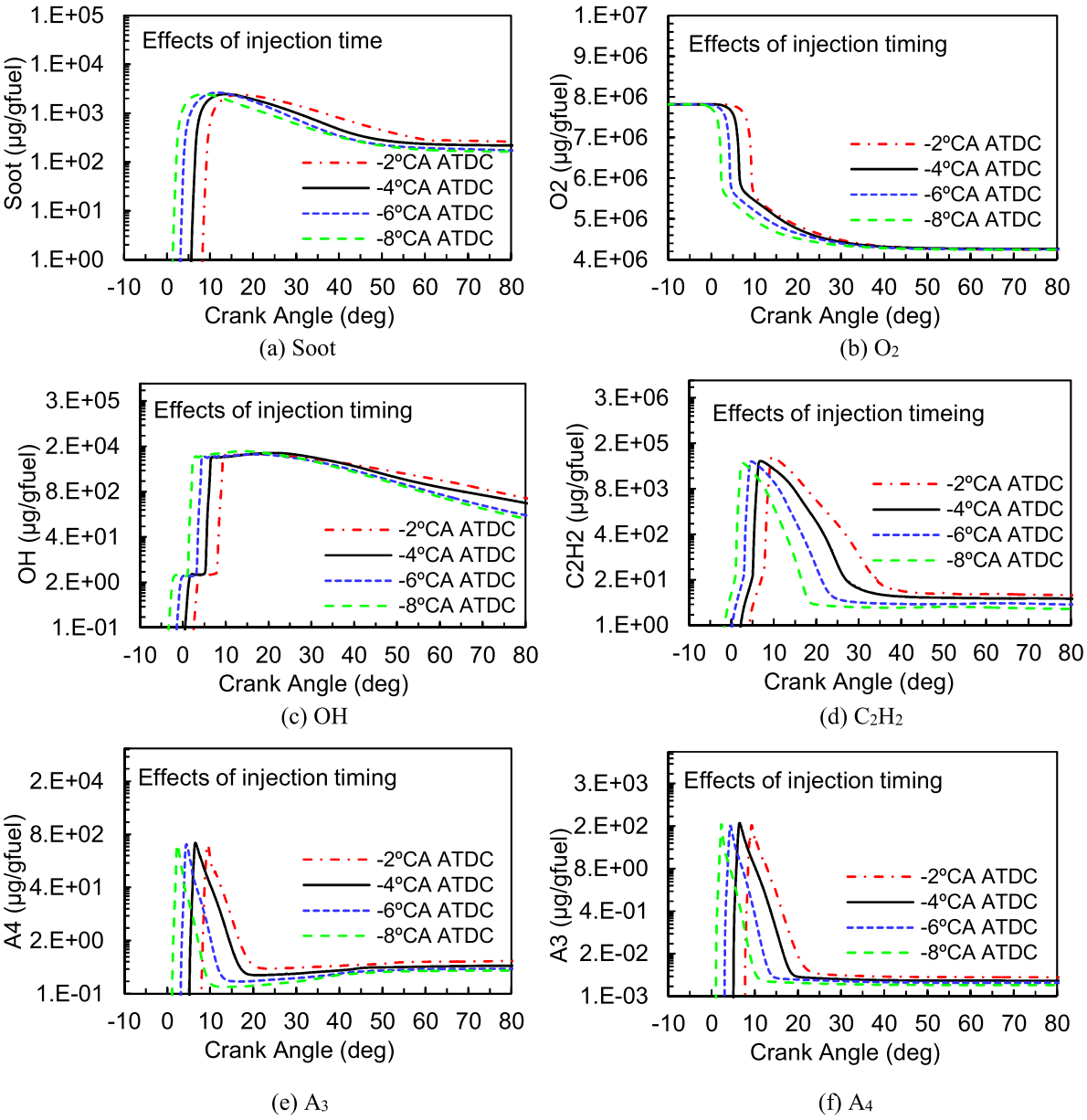

Fig. 7. The simulated soot, O_2, C_2H_2, OH, A_3 and A_4 of the diesel engine fuelled with ABE20 under various injection timings.

injection timing as illustrated in Fig. (e).

4.2. The effects of the EGR ratio on combustion and emission characteristics of the diesel engine

This section was mainly investigated the effect of the EGR ratio on the combustion and emissions characteristics of the diesel engine fuelled with ABE20. Fig. 9 displays the simulated in-cylinder pressure, HRR and in-cylinder mean temperature of the diesel engine fuelled with the ABE20 under different EGR ratios (0%, 15%, 25% and 35%). It is worthwhile to note that the EGR was presented by the carbon dioxide (CO_2) in the engine simulation. As can be seen from Fig. 9, the peak combustion pressure, peak heat release rate, and in-cylinder temperature were decreased with increasing the EGR ratio, and the combustion phasing was also retarded. These trends were mainly attributed to the following reasons. First, with increasing the EGR ratio, the volume ratio of the CO_2 was increased in the cylinder, which would dilute the mixture and reduce the chemical reaction rate. In addition, the chemical effect of the CO_2 would also suppress and even alter the chemical equilibrium of the CO + OH═CO_2+H and CO + O_2═CO_2+O, while the CO + OH═CO_2+H was the main reaction route for the CO [48], and would release a large amount of heat during the reaction process. Furthermore, the combustion rate and combustion efficiency were also affected with introducing the EGR. Therefore, the peak heat release rate and in-cylinder mean temperature were decreased with increasing the EGR ratio, which in turn effected the peak combustion pressure. Moreover, the CO_2 is the triatomic molecule, and has a relative high specific heat capacity, which means that the increase of the in-cylinder mean temperature was limited with increasing the EGR ratio.

Fig. 10 illustrates the soot, NOx, CO and HC emissions of the diesel engine fuelled with the ABE20 under different EGR ratios. It can be seen from Fig. 10 (a), the soot mass was increased with

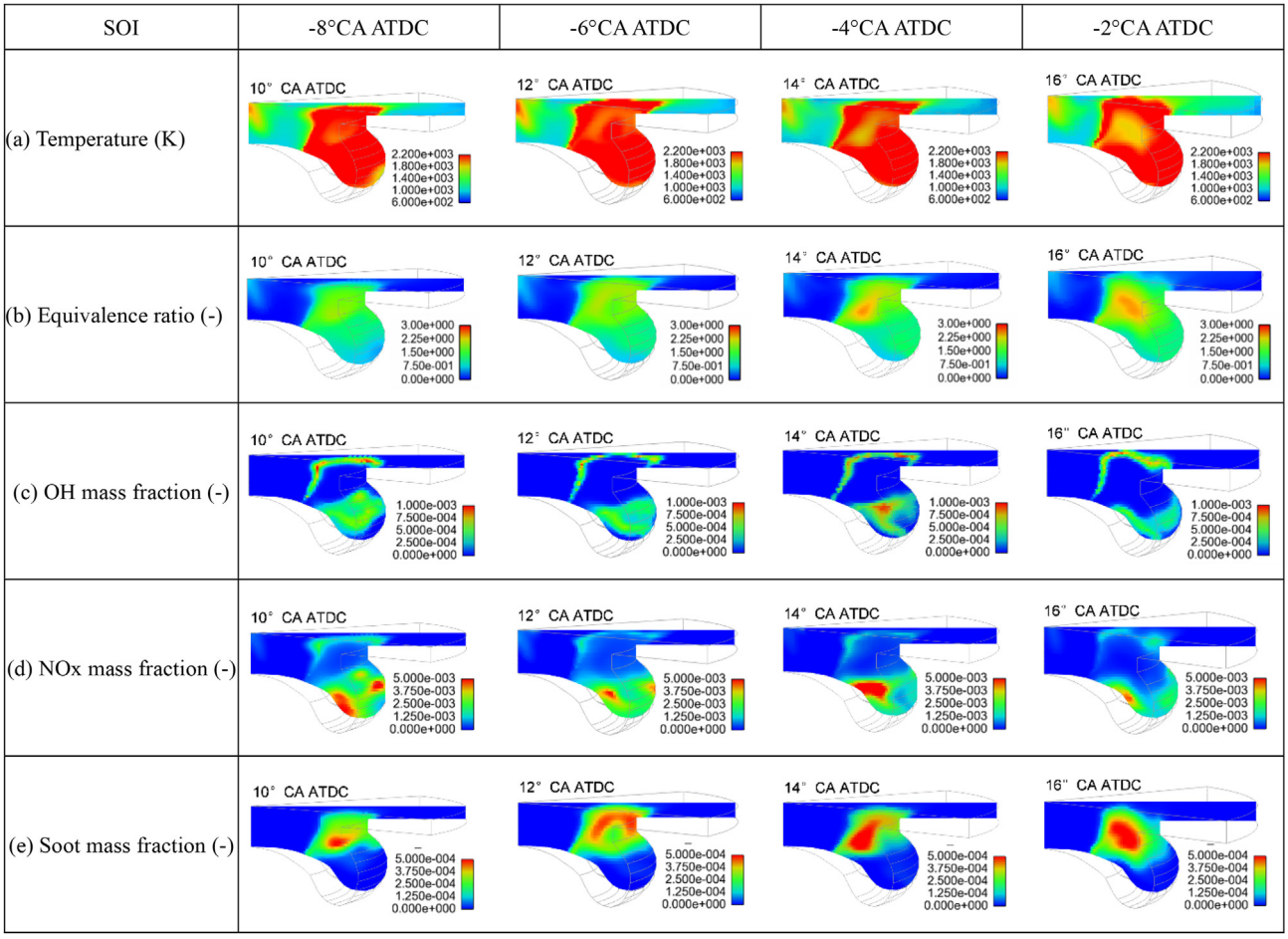

Fig. 8. The effects of the injection timing on the simulated temperature, equivalent ratio, OH, NOx and soot distribution of the diesel engine fuelled with ABE20.

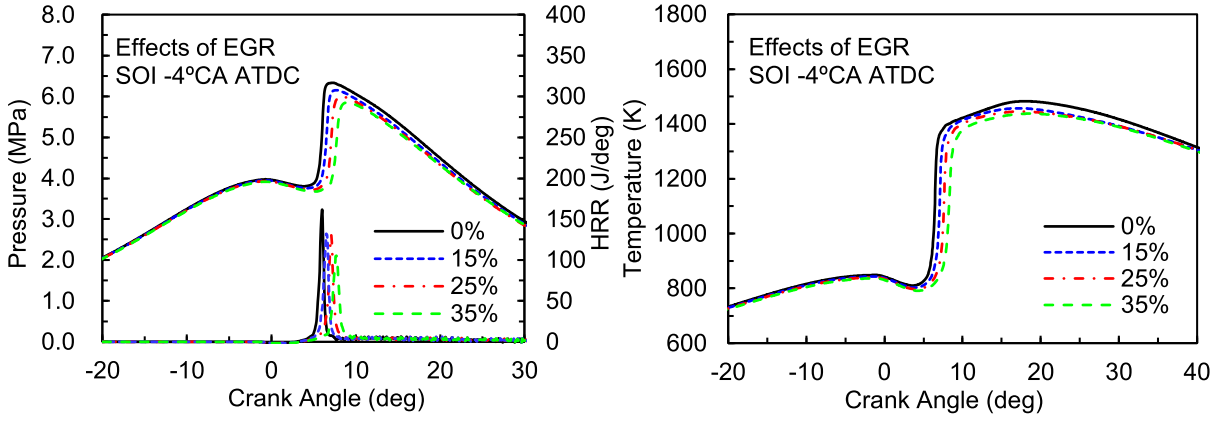

(a) In-cylinder pressure and heat release rate

(b) In-cylinder mean temperature

Fig. 9. The in-cylinder pressure, heat release rate, tempeature of the diesel engine fuelled under different EGR ratios.

increasing the EGR ratio, while the NOx emissions were declined with increasing the EGR ratio. This is because that the in-cylinder mean temperature was decreased with using the EGR as shown in Fig. 9 (b). As stated earlier, the formation of the NOx emissions in the cylinder was strongly depended on the combustion temperature. With decreasing the temperature in the cylinder, the activation energy of the reactions related to the NOx formation was increased, and thus the NOx emissions were decreased in the cylinder. However, the soot oxidation was limited with increasing the EGR due to its dilution and chemical effects. As one can see from Fig. 10 (b), the CO and HC emissions were increased with the EGR ratio. With increasing EGR ratio, the chemical effect of the CO_2 was intensified, and thereby affecting the reactions of the CO + OH═ CO_2+H and CO + O_2═CO_2+O. Thus, the CO emission was increased

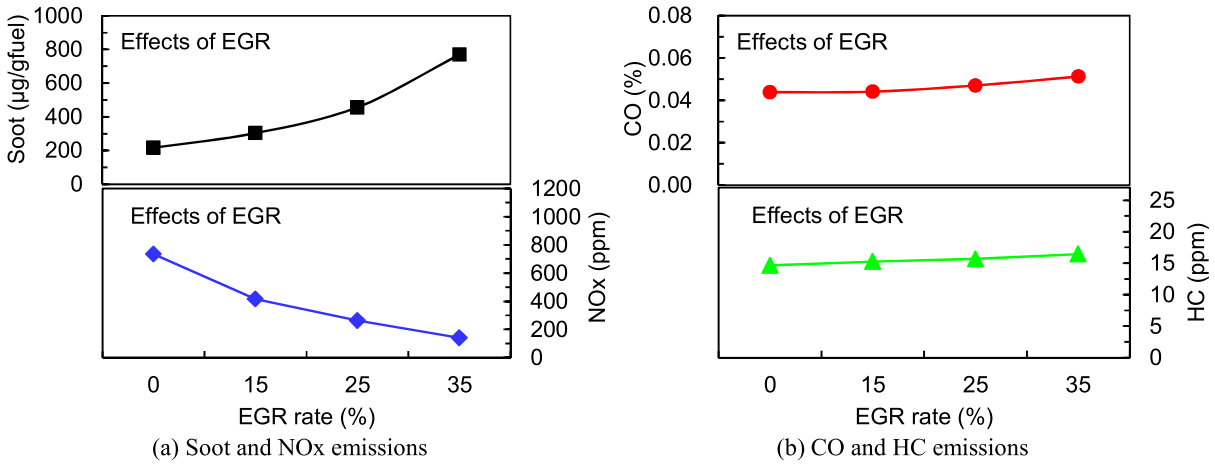

Fig. 10. The soot, NOx, CO and HC of the diesel engine fuelled with ABE20 under different EGR ratios.

with the EGR ratio. Additionally, the combustion efficiency of the diesel engine was decreased because the combustion flame was easily quenched near the wall of the cylinder with using the EGR, which became the main source of the HC emissions [49]. Furthermore, although using the ABE20 in the diesel engine increased the oxygen concentration, the HC oxidation rate was significantly affected with the decrease of the in-cylinder temperature.

Fig. 11 demonstrates the simulated soot, O_2, OH, C_2H_2, A_3 and A_4 of the diesel engine fuelled with the ABE20 under different EGR ratios. Overall, the soot and intermediate species formation of the test engine were retarded with increasing the EGR ratio, and the final production of each intermediate species increased with increasing the EGR ratio. Specifically, the generation rate of the soot decreased, while the final peak soot mass slightly increased with the increase of the EGR ratio as illustrated in Fig. 11 (a). These trends were mainly attributed to the following reasons. First, with introducing the EGR in the cylinder, the ignition delay period of the diesel engine fuelled with the ABE20 were retarded and the heat release rate was also decreased as illustrated in Fig. 9. That meant the auto-ignition timing of the mixture was delayed with importing the EGR [50]. Therefore, the intermediate species, soot precursors and final soot formation of the diesel engine fuelled with the ABE20 were delayed with increasing the EGR ratio. Second, with increasing reaction time, more intermediate species, soot precursors and final soot were formed and accumulated. However, the consumption rates of the intermediate species, soot precursors and final soot were greatly decreased with increasing the EGR ratio due to the reduction of the combustion temperature. Third, the activation energy of the consumption reactions related to the intermediate species, soot precursors and final soot were increased due to the lower combustion temperature. Moreover, the oxidation rates of the soot precursors and final soot were limited with increasing the EGR due to its dilution and chemical effects. Accordingly, with increasing the EGR ratio, the generation rate of the OH radical and its peak mass decreased significantly due the reduction of the in-cylinder temperature as displayed in Fig. 11(c). Therefore, the effect of the OH radical on the soot oxidation was weakened, resulting in increasing the soot emissions. In addition, as illustrated in Fig. 11 (b), the concentration of the O_2 was diluted due to the introduction of EGR in the cylinder, which also led to the soot formation and greatly affected the soot oxidation. Furthermore, the formation of the soot precursors of the C_2H_2, A_3 and A_4 increased with the increase of the EGR ratio, and their oxidation process also limited by the EGR. The results were mainly attributed to the following reasons. On the one hand, the combustion temperature was decreased with increasing the EGR ratio, which limited the OH radical generation, and thereby affecting the oxidation of the C_2H_2, A_3 and A_4. In addition, the EGR also diluted the mixture in the cylinder, and greatly reduced the reactions concentration, which decreased the effect of the air entrainment produced by the fuel spray, and caused the rich mixture along the fuel spray, resulting in increasing the soot and intermediate species formation. These pollutants could also evolve over time [51].

Fig. 12 presents the simulated temperature, equivalent ratio, OH, NOx and soot distribution in the cylinder of the diesel engine fuelled with the ABE20 under different EGR ratios. As stated earlier, the cross-sectional planes were cut at the timing of the peak soot mass formation during the simulation. As can be seen from Fig. 12 (a), with increasing the EGR ratio, the combustion temperature was decreased, and became unevenly distribution in the cylinder. In addition, the combustion took place at the end of the fuel spray due to the earlier formed premixed mixture and the appropriate the equivalence ratio (as displayed in Fig. 12 (b)). Obviously, with the spray combustion development, the OH radical was generated around the flame. Without introducing EGR, the concentration of the OH radical was apparently higher than that of using EGR ratio as illustrated in Fig. 12 (c). Furthermore, with increasing the EGR ratio, the concentration of the OH radial decreased due to the reduction of the combustion temperature. Fortunately, the NOx emissions were obviously decreased with increasing the EGR due to the decrease of the peak combustion temperature (as depicted in Fig. 12 (d)). In addition, most of the NOx emissions were formed inside the high temperature zone, particularly in the piston bowl due to the fuel spray penetration, impingement and interaction with the wall. Although, the soot emissions were high in the earlier stage during the combustion process without EGR, the final soot emissions, however, were increased with increasing the EGR ratio, and mainly located in the piston bowl as demonstrated in Fig. 12 (e). It is largely due to the relatively high concentration of the OH radical and free of the dilution effect of the EGR, which greatly promoted the soot oxidation without introducing EGR. On the contrary, with using the EGR, the concentration of the OH radical decreased and limited the soot oxidation through the reaction of $C(s) + OH{=}CO + 1/2H_2$. In addition, the reaction rate of $C(s) + OH{=}CO + 1/2H_2$ was decreased due to the dilution and chemical effects of the EGR.

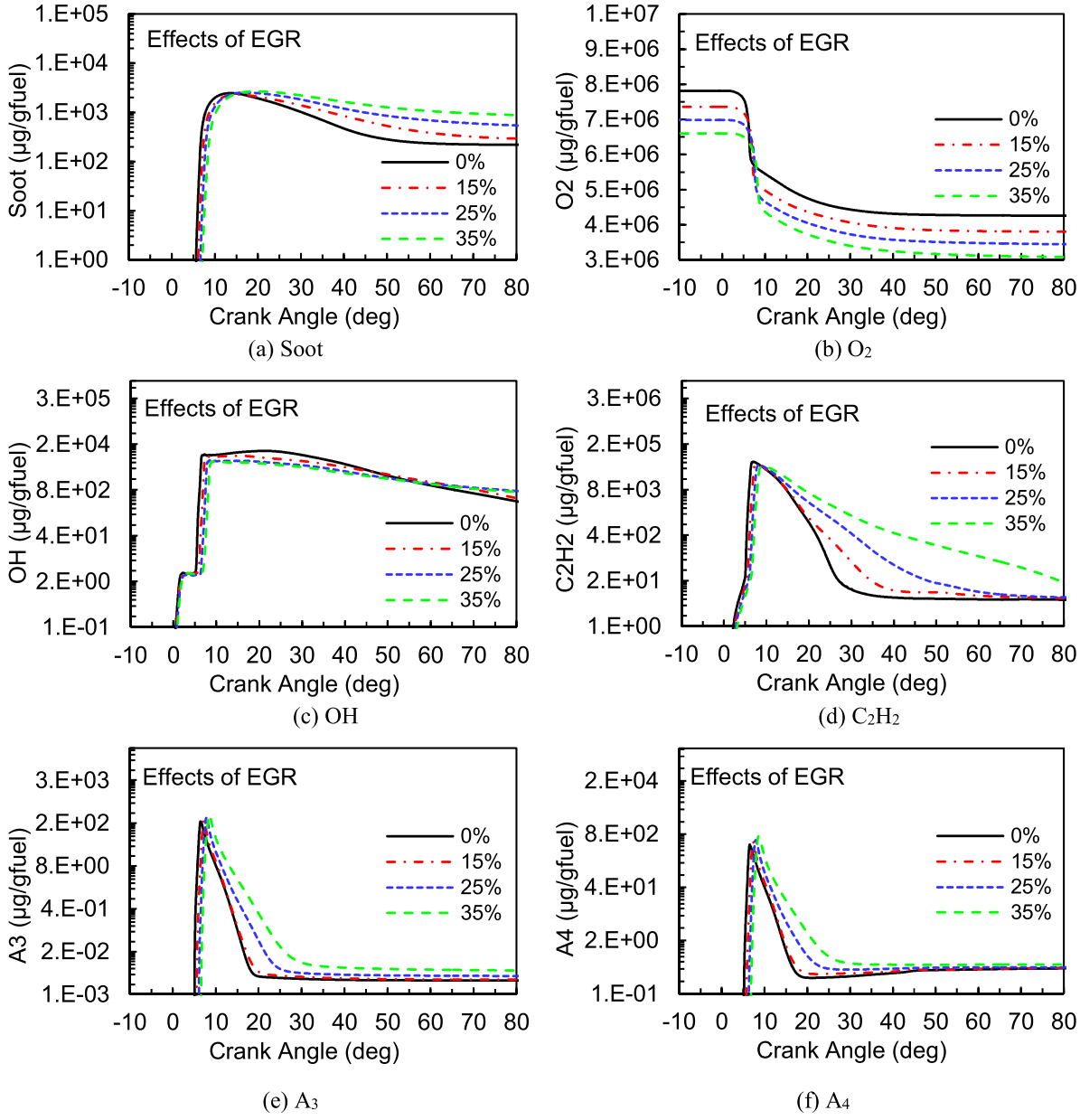

Fig. 11. The simulated soot, O_2, C_2H_2, OH, A_3 and A_4 of the diesel engine fuelled with ABE20 under different EGR ratios.

5. Conclusions

In this paper, the D100, ABE10 and ABE20 were tested on the diesel engine under different injection timing for obtaining the in-cylinder pressure and emissions data. Then the sector computational domain of the diesel engine was built through the CFD KIVA-3V code coupled with the open-source CANTERA chemical kinetics code by replacing the KIVA default chemical subroutines, and validated against with the experimental data. Last, the effects of the injection timing and EGR rate on combustion and emission characteristics of the diesel engine fuelled with ABE20 were investigated on the calibrated simulation model. The main conclusions were presented as follows:

(1) The peak combustion pressure and peak heat release rate of the test diesel engine fuelled with the ABE20 were increased and their locations were advanced with the advance of the fuel injection timing. The heat release rate was advanced with the earlier injection timing. In addition, the soot, CO and HC emissions of the diesel engine fuelled with the ABE20 were decreased with advancing the injection timing, while the NOx emissions were increased with advancing the injection timing. Furthermore, the intermediate species and soot precursors of the diesel engine fuelled with the ABE20 were advanced with using the earlier injection timing.

(2) The peak combustion pressure, peak heat release rate, and in-cylinder temperature were decreased, and the combustion phasing was retarded with increasing the EGR ratio. In addition, the soot, CO and HC emissions were increased with increasing the EGR ratio, while the NOx emissions were declined with increasing the EGR ratio. The intermediate species and soot precursors of the diesel engine fuelled with the ABE20 were retarded with increasing the EGR ratio,

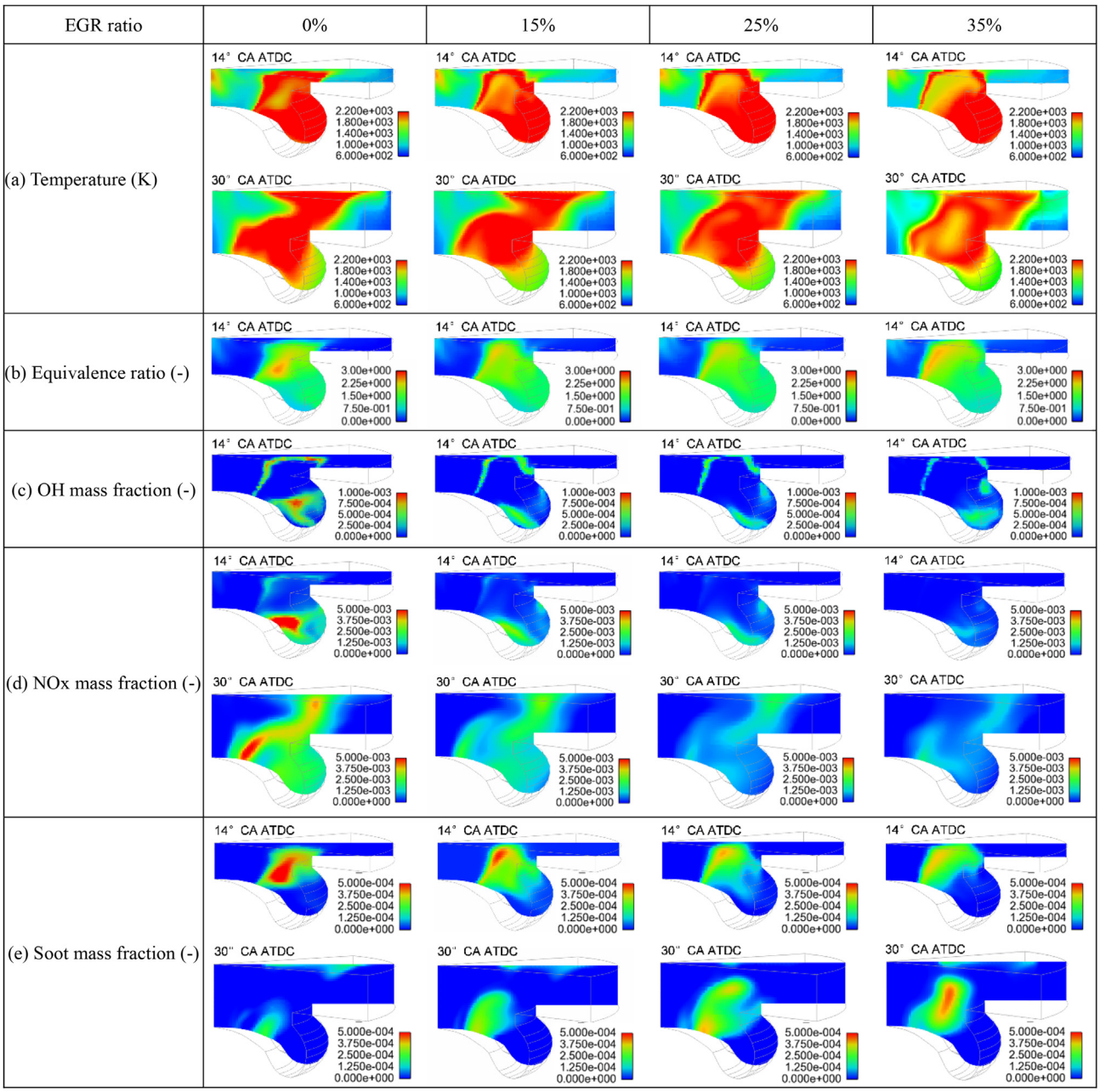

Fig. 12. The impacts of the EGR on the simulated temperature, equivalent ratio, OH, NOx and soot distribution of the diesel engine fuelled with ABE20.

while the final production of each intermediate species increased with increasing the EGR ratio.

(3) The high combustion temperature regions of the diesel engine fuelled with the ABE20 were located near the piston bowl due to the fuel spray penetration, initial premixed mixture formation, and the late combustion occurred.

(4) Most of the NOx emissions were formed inside the high temperature zone, particularly in the piston bowl due to the fuel spray penetration, impingement and interaction with the wall. Although, the soot emissions were high in the earlier stage during the combustion process without EGR, the final soot emissions, however, were increased with increasing the EGR ratio, and mainly located in the piston bowl.

Author contributions

Xiongbo Duan: Methodology, Software, Validation, Project administration, Funding acquisition, Writing – original draft. Zhengxin Xu: Conceptualization, Software, Validation, Writing – review & editing. Banglin Deng: Data curation. Jingping Liu: Formal analysis.

Declaration of competing interest

The authors declare that they have no known competing financial interests or personal relationships that could have appeared to influence the work reported in this paper.

Acknowledgements

This research paper is mainly sponsored by the Science and Technology Innovation Program of Hunan Province, China (Grant No. 2020RC2025) and the Natural Science Foundation of Hunan Province, China (Grant No. 2020JJ5071). The authors appreciate the anonymous reviewers and the editor for carefully reading and providing many constructive comments and suggestions to improve the manuscript.

Abbreviation

ICE	internal combustion engine
CN	cetane number
ABE	acetone–butanol–ethanol
PAHs	polycyclic aromatic hydrocarbons
LTC	low temperature combustion
HCCI	Homogeneous charge compression ignition
NOx	nitrogen oxide
ECU	electronic control unit
HC	hydrocarbon
CO	carbon monoxide
EGR	exhaust gas recirculation
JSR	jet-stirred reactors
ULSD	ultra-low sulfur diesel
TDC	top dead center
BDC	bottom dead center
IVC	intake valve closing
ATDC	after top dead center
TDC	top dead center
EVO	exhaust valve opening
CFD	computational fluid dynamics
HRR	heat release rate
CO_2	carbon dioxide

References

[1] Mock P. CO2 emission standards for passenger cars and light-commercial vehicles in the European Union. ICCT Policy Update; 2019.
[2] Duan X, Liu J, Tan Y, Luo B, Guo G, Wu Z, et al. Influence of single injection and two-stagnation injection strategy on thermodynamic process and performance of a turbocharged direct-injection spark-ignition engine fuelled with ethanol and gasoline blend. Appl Energy 2018;228:942–53.
[3] Liu J, Dumitrescu CE. Flame development analysis in a diesel optical engine converted to spark ignition natural gas operation. Appl Energy 2018;230:1205–17.
[4] Abdellatief TMM, Ershov MA, Kapustin VM. New recipes for producing a high-octane gasoline based on naphtha from natural gas condensate. Fuel 2020;276:118075.
[5] Ershov MA, Klimov NA, Burov NO, Abdellatief TMM, Kapustin VM. Creation a novel promising technique for producing an unleaded aviation gasoline 100UL. Fuel 2021;284:118928.
[6] Liu J, Dumitrescu CE. Numerical investigation of methane number and wobbe index effects in lean-burn natural gas spark-ignition combustion. Energy Fuels 2019;33:4564–74.
[7] Li Y, Wang S, Duan X, Liu S, Liu J, Hu S. Multi-objective energy management for Atkinson cycle engine and series hybrid electric vehicle based on evolutionary NSGA-II algorithm using digital twins. Energy Convers Manag 2021;230:113788.
[8] Liu H, Zhang P, Li Z, Luo J, Zheng Z, Yao M. Effects of temperature inhomogeneities on the HCCI combustion in an optical engine. Appl Therm Eng 2011;31:2549–55.
[9] Yin X, Li Z, Yang B, Sun T, Wang Y, Zeng K. Experimental study of the combustion characteristics prediction model for a sensor-less closed-loop control in a heavy-duty NG engine. Fuel 2021;300:120945.
[10] Sadeghinezhad E, Kazi S, Sadeghinejad F, Badarudin A, Mehrali M, Sadri R, et al. A comprehensive literature review of bio-fuel performance in internal combustion engine and relevant costs involvement. Renew Sustain Energy Rev 2014;30:29–44.
[11] Lee TH, Hansen AC, Li G, Lee T. Effects of isopropanol-butanol-ethanol and diesel fuel blends on combustion characteristics in a constant volume chamber. Fuel 2019;254:115613.
[12] Ershov M, Potanin D, Gueseva A, Abdellatief TMM, Kapustin V. Novel strategy to develop the technology of high-octane alternative fuel based on low-octane gasoline Fischer-Tropsch process. Fuel 2020;261:116330.
[13] Chen Z, Wang L, Zhang Q, Zhang X, Yang B, Zeng K. Effects of spark timing and methanol addition on combustion characteristics and emissions of dual-fuel engine fuelled with natural gas and methanol under lean-burn condition. Energy Convers Manag 2019;181:519–27.
[14] Duan X, Liu J, Yuan Z, Guo G, Liu Q, Tang Q, et al. Experimental investigation of the effects of injection strategies on cycle-to-cycle variations of a DISI engine fueled with ethanol and gasoline blend. Energy 2018;165:455–70.
[15] Li Y, Duan X, Liu Y, Liu J, Guo G, Tang Y. Experimental investigation the impacts of injection strategies coupled with gasoline/ethanol blend on combustion, performance and emissions characteristics of a GDI spark-ignition engine. Fuel 2019;256:115910.
[16] Szwaja S, Naber JD. Combustion of n-butanol in a spark-ignition IC engine. Fuel 2010;89:1573–82.
[17] Ma Y, Huang R, Huang S, Zhang Y, Xu S, Wang Z. Experimental investigation on the effect of n-pentanol blending on spray, ignition and combustion characteristics of waste cooking oil biodiesel. Energy Convers Manag 2017;148:440–55.
[18] Li Y, Chen Y, Wu G. A new skeletal mechanism for diesel-n-butanol blends combustion in engine. Fuel 2020;264:116856.
[19] Green EM. Fermentative production of butanol—the industrial perspective. Curr Opin Biotechnol 2011;22:337–43.
[20] Ikegami T, Negishi H, Nakayama S, Kobayashi G, Sakaki K. Pervaporative concentration of biobutanol from ABE fermentation broths by Clostridium saccharoperbutylacetonicum using silicone rubber-coated silicalite-1 membranes. Separ Purif Technol 2014;132:206–12.
[21] Chang Y-C, Lee W-J, Wu TS, Wu C-Y, Chen S-J. Use of water containing acetone–butanol–ethanol for NOx-PM (nitrogen oxide-particulate matter) trade-off in the diesel engine fueled with biodiesel. Energy 2014;64:678–87.
[22] Patraşcu I, Bîldea CS, Kiss AA. Eco-efficient butanol separation in the ABE fermentation process. Separ Purif Technol 2017;177:49–61.
[23] Wu H, Nithyanandan K, Zhou N, Lee TH, Lee C-fF, Zhang C. Impacts of acetone on the spray combustion of Acetone–Butanol–Ethanol (ABE)-Diesel blends under low ambient temperature. Fuel 2015;142:109–16.
[24] Bellido C, Lucas S, González-Benito G, García-Cubero MT, Coca M. Synergistic positive effect of organic acids on the inhibitory effect of phenolic compounds on Acetone-Butanol-Ethanol (ABE) production. Food Bioprod Process 2018;108:117–25.
[25] Tang Q, Duan X, Liu Y, Li S, Zhao Z, Ren K, et al. Experimental study the effects of acetone–butanol–ethanol (ABE), spark timing and lambda on the performance and emissions characteristics of a high-speed SI engine. Fuel 2020;279:118499.
[26] Fournier S, Simon G, Seers P. Evaluation of low concentrations of ethanol, butanol, BE, and ABE blended with gasoline in a direct-injection, spark-ignition engine. Fuel 2016;181:396–407.
[27] Zhang H, Li S, Jiao Y, Emil iojoiu E, Da Costa P, Elena Galvez M, et al. Structure, surface and reactivity of activated carbon: from model soot to Bio Diesel soot. Fuel 2019;257:116038.
[28] Wang H, Frenklach M. A detailed kinetic modeling study of aromatics formation in laminar premixed acetylene and ethylene flames. Combust Flame 1997;110:173–221.
[29] Pitz WJ, Mueller CJ. Recent progress in the development of diesel surrogate fuels. Prog Energy Combust Sci 2011;37:330–50.
[30] Raj A, Prada IDC, Amer AA, Chung SH. A reaction mechanism for gasoline surrogate fuels for large polycyclic aromatic hydrocarbons. Combust Flame 2012;159:500–15.
[31] Sharma S, Green WH. Computed rate coefficients and product yields for c-C5H5 + CH3 → Products. J Phys Chem 2009;113:8871–82.
[32] Veza I, Said MFM, Latiff ZA. Progress of acetone-butanol-ethanol (ABE) as biofuel in gasoline and diesel engine: a review. Fuel Process Technol 2019;196:106179.
[33] Rao DCK, Karmakar S, Som S. Puffing and micro-explosion behavior in combustion of butanol/Jet A-1 and acetone-butanol-ethanol (ABE)/Jet A-1 fuel droplets. Combust Sci Technol 2017;189:1796–812.
[34] Zhou N, Huo M, Wu H, Nithyanandan K, Lee C-fF, Wang Q. Low temperature spray combustion of acetone–butanol–ethanol (ABE) and diesel blends. Appl Energy 2014;117:104–15.
[35] Hasan MM, Rahman MM. Homogeneous charge compression ignition combustion: advantages over compression ignition combustion, challenges and solutions. Renew Sustain Energy Rev 2016;57:282–91.
[36] Duan X, Lai M-C, Jansons M, Guo G, Liu J. A review of controlling strategies of the ignition timing and combustion phase in homogeneous charge compression ignition (HCCI) engine. Fuel 2021;285:119142.
[37] Duan X, Liu Y, Liu J, Lai M-C, Jansons M, Guo G, et al. Experimental and numerical investigation of the effects of low-pressure, high-pressure and internal EGR configurations on the performance, combustion and emission characteristics in a hydrogen-enriched heavy-duty lean-burn natural gas SI engine. Energy Convers Manag 2019;195:1319–33.
[38] Rakopoulos C, Dimaratos A, Giakoumis E, Rakopoulos D. Study of turbocharged diesel engine operation, pollutant emissions and combustion noise radiation during starting with bio-diesel or n-butanol diesel fuel blends. Appl Energy 2011;88:3905–16.
[39] Lapuerta M, García-Contreras R, Campos-Fernández J, Dorado MP. Stability, lubricity, viscosity, and cold-flow properties of alcohol– diesel blends. Energy

Fuels 2010;24:4497–502.
[40] Amsden AA. KIVA-3V, release 2: improvements to KIVA-3V. NM (US): Los Alamos National Lab.; 1999.
[41] Goodwin DG. An open-source, extensible software suite for CVD process simulation. Chemical Vapor Deposition XVI & Eurocvd 2003;14(40):2003–8.
[42] Xu Z, Duan X, Liu Y, Deng B, Liu J. Spray combustion and soot formation characteristics of the acetone-butanol-ethanol/diesel blends under diesel engine-relevant conditions. Fuel 2020;280:118483.
[43] Han Z, Reitz RD. Turbulence modeling of internal combustion engines using RNG κ-ε models. Combust Sci Technol 1995;106:267–95.
[44] O'Rourke PJ, Amsden AA. The TAB method for numerical calculation of spray droplet breakup. SAE Technical Paper; 1987.
[45] O'Rourke PJ. Collective drop effects on vaporizing liquid sprays. University of Princeton; 1981.
[46] Zeng YB, Lee CF. A preferential vaporization model for multicomponent droplets and sprays. Atomization Sprays 2002;12:163–86.
[47] Fenimore CP, Jones GW. Oxidation of soot by hydroxyl radicals. J Phys Chem 1967;71:593–7.
[48] Duan X, Li Y, Liu Y, Zhang S, Guan J, Lai M-C, et al. Dilution gas and hydrogen enrichment on the laminar flame speed and flame structure of the methane/air mixture. Fuel 2020;281:118794.
[49] Han D, E J, Deng Y, Chen J, Leng E, Liao G, et al. A review of studies using hydrocarbon adsorption material for reducing hydrocarbon emissions from cold start of gasoline engine. Renew Sustain Energy Rev 2021;135:110079.
[50] Liang J, Xiao D, Zhang Q, Chen Z, Zheng Z. Combined impact of alcohol-fuel properties on performance and emissions characteristics with low-temperature combustion in a diesel engine. J Energy Eng 2021;147:04021018.
[51] Deng B, Chen Y, Duan X, Li D, Li Q, Tao D, et al. Dispersion behaviors of exhaust gases and nanoparticle of a passenger vehicle under simulated traffic light driving pattern. Sci Total Environ 2020;740:140090.